Safety, Biodistribution, and Dosimetry of ^{99m}Tc-HYNIC-Annexin V, a Novel Human Recombinant Annexin V for Human Application

Gerrit J. Kemerink, PhD[1]; Xuan Liu, PhD[2]; Davy Kieffer[3]; Sarah Ceyssens[2]; Luc Mortelmans, MD, PhD[2]; Alfons M. Verbruggen, PhD[3]; Neil D. Steinmetz, MD, PhD[4]; Jean-Luc Vanderheyden, PhD[4]; Allan M. Green, MD, PhD[4]; and Kristin Verbeke, PhD[3]

[1]Department of Nuclear Medicine, University Hospital Maastricht, Maastricht, The Netherlands; [2]Department of Nuclear Medicine, University Hospital Gasthuisberg, Leuven, Belgium; [3]Laboratory of Radiopharmaceutical Chemistry, Faculty of Pharmaceutical Sciences, University of Leuven, Leuven, Belgium; and [4]Theseus Imaging Corporation, Boston, Massachusetts

^{99m}Tc-hydrazinonicotinamido (HYNIC)–annexin V is a novel tracer for in vivo imaging of apoptosis. The present study on humans was performed to investigate the safety of ^{99m}Tc-HYNIC-annexin V and to quantify the biodistribution and radiation dose. **Methods:** Six healthy, male volunteers participated in the study. A dual-head gamma camera was used to acquire conjugate anterior and posterior views. Imaging started with a transmission scan using a ^{57}Co-flood source to obtain a map of the local thickness of the volunteer. Approximately 250 MBq of ^{99m}Tc-HYNIC-annexin V were injected intravenously, directly followed by a 30-min dynamic study. Whole-body scans were obtained at about 30 min, 3 h, 6 h, and 24 h after injection. Organ uptake was determined after correction for background, scatter, and attenuation. The MIRDOSE3.1 program was used to calculate organ-absorbed doses and effective dose. Signs of adverse effects were investigated by monitoring renal and liver function, hematology, blood coagulation, and vital signs (blood pressure, pulse, respiration rate, temperature, and electrocardiogram). **Results:** The kidneys accumulated 49.7 ± 8.1 percentage injected dose (%ID) at 3 h after injection; the liver, 13.1 ± 1.0 %ID; the red marrow, 9.2 ± 1.8 %ID; and the spleen, 4.6 ± 1.6 %ID. More than 90% of the blood activity was cleared with a half-life of 24 ± 3 min. The biologic half-life of the activity registered over the total body was long (69 ± 7 h). Excretion of the activity was almost exclusively through the urine (22.5 ± 3.5 %ID at 24 h), and hardly any activity was seen in the bowel or feces. Absorbed doses were found to be 196 ± 31 μGy/MBq for the kidneys, 41 ± 12 μGy/MBq for the spleen, 16.9 ± 1.3 μGy/MBq for the liver, and 8.4 ± 0.9 μGy/MBq for the red marrow. The effective dose was 11.0 ± 0.8 μSv/MBq, or 2.8 ± 0.2 mSv for the average injected activity of 250 MBq. No adverse effects were observed. **Conclusion:** ^{99m}Tc-HYNIC-annexin V is a safe radiopharmaceutical, having a favorable biodistribution for imaging of apoptosis in the abdominal as well as thoracic area with an acceptable radiation dose.

Key Words: biosafety; biodistribution; radiation dosimetry; apoptosis; annexin V

J Nucl Med 2003; 44:947–952

Apoptosis or programmed cell death plays an important role in embryogenesis and homeostasis, and abnormal induction or inhibition of apoptosis has been related to several diseases (*1*,*2*). As a consequence, in vivo imaging of apoptosis has potentially numerous valuable applications, as can be seen in the rapidly growing body of literature on this subject (*2*–*4*). A general and persistent feature characterizing cells undergoing apoptosis is the rapid exposure of phosphatidylserine, a membrane-bound phospholipid, by transport from the inner to the outer leaflet of the plasma membrane (*5*). This phenomenon occurs early in the apoptotic process, before membrane bleb formation and DNA fragmentation, forming an attractive target for visualization of apoptosis. Annexin V (AnxV), a 36-kDa human protein, binds with high affinity (dissociation constant = 7 nmol) to phosphatidylserine (*6*,*7*), and fluorescein-labeled AnxV derivatives have been widely used for in vitro visualization of apoptosis. More recently, ^{99m}Tc-labeled AnxV derivatives have been proposed as tracers for in vivo application.

Up to now, two ^{99m}Tc-labeled AnxV compounds have been studied in humans, differing in the bifunctional chelating agent used for complexation of ^{99m}Tc (*8*–*10*). In ^{99m}Tc-i-AnxV (Mallinckrodt), AnxV was derivatized with a monodentate n-1-imino-4-mercaptobutyryl side chain (*9*), whereas in ^{99m}Tc-BTAP-AnxV (Apomate; Theseus Imaging Corp.), the protein is modified with an N2S2 bis(mercaptoacetyl)diaminopentanoyl group (*10*). The radiochemical purity (82% ± 12%) and stability of ^{99m}Tc-i-AnxV were found to be suboptimal, probably because the bifunctional ligand is only monodentate. In contrast, ^{99m}Tc-BTAP-AnxV is a stable and well-defined ^{99m}Tc-complex but has to be pre-

Received Oct. 24, 2002; revision accepted Feb. 13, 2003.

For correspondence or reprints contact: Gerrit J. Kemerink, PhD, Department of Nuclear Medicine, University Hospital Maastricht, P.O. Box 5800, 6202 AZ Maastricht, The Netherlands.

E-mail: gkk@rdia.azm.nl

pared through a preformed chelate approach that is time consuming and labor intensive. In addition, the biologic behavior of these radiolabeled AnxV derivatives was found to be influenced by the choice of the ligand used for complexation of ^{99m}Tc. ^{99m}Tc-i-AnxV was found to have a long biologic half-life of 62 ± 13 h, and ^{99m}Tc-BTAP-AnxV was found to have a much shorter one of 16 ± 7 h. After intravenous administration of these tracers, about 75% of the injected dose was eliminated through the urine and 25% through the feces. However, in the case of ^{99m}Tc-BTAP-AnxV, activity had already appeared in the bowel within a few hours, probably precluding imaging of apoptosis in the abdomen.

Recently, a ^{99m}Tc-labeled AnxV derivative has been described in which the protein is modified with a hydrazinonicotinamide side chain (^{99m}Tc-hydrazinonicotinamido [HYNIC]–AnxV) (*11*,*12*). HYNIC-AnxV can easily be labeled with ^{99m}Tc by simple addition of Sn^{2+} ions and pertechnetate in the presence of tricine as coligand and results in preparations with radiochemical yields exceeding 90% in only 15 min. Biodistribution studies on normal rats have indicated that ^{99m}Tc-HYNIC-AnxV is excreted mainly through the kidneys. This excretion route, since it might allow visualization of apoptosis in the abdomen, gives ^{99m}Tc-HYNIC-AnxV a clear advantage over ^{99m}Tc-BTAP-AnxV. In addition, Ohtsuki et al. (*12*) obtained promising results using ^{99m}Tc-HYNIC-AnxV in animal models of apoptosis including anti-Fas-mediated hepatic apoptosis, rejection of allogeneic heterotopic cardiac allografts, cyclophosphamide treatment of murine lymphoma, cyclophosphamide-induced apoptosis in bone marrow, and leukocyte apoptosis associated with abscess formation (*11*–*14*).

The aim of the present study was to evaluate ^{99m}Tc-HYNIC-AnxV for the first time in humans in a phase I study. The major objectives of the study were to determine the safety and tolerability of a single dose of ^{99m}Tc-HYNIC-AnxV, to determine the biodistribution of ^{99m}Tc-HYNIC-AnxV in healthy, male volunteers, and to determine the radiation dose in healthy volunteers.

MATERIALS AND METHODS

Subjects

Six young and healthy male volunteers participated in a study that was approved by the local ethics committee. Informed consent was obtained from all volunteers.

Radioactive Tracer

Good manufacturing practice–grade human recombinant AnxV was provided by Theseus Imaging Corp. and conjugated with hydrazinonicotinamide according to the procedure described by Ohtsuki et al. (*12*). Labeling with ^{99m}Tc was performed by consecutive addition of 24 μg of $SnCl_2 \cdot 2H_2O$ in 0.05 mol/L HCl, 15 μL of tricine solution (100 mg/mL in 20 mmol/L citrate buffer, pH 5.2), and 1.11 GBq of $^{99m}TcO_4^-$ to a vial containing 60 μg of the modified protein in 100 μL of citrate buffer (20 mmol/L, pH 5.2). Radiochemical purity was assessed by thin-layer chromatography on instant thin-layer chromatography strips (Gelman Sciences) using acetone as the mobile phase for determination of the percentage of $^{99m}TcO_4^-$ and acid citrate dextrose (68 mmol/L dextrose, 74 mmol/L citrate, pH 5.0) for determination of the overall radiochemical purity. Before injection, the preparation was passed through a sterile 0.22-μm filter. Each volunteer was injected with 250–370 MBq of ^{99m}Tc-HYNIC-AnxV.

Data Acquisition

Imaging was performed on a dual-head gamma camera with low-energy high-resolution collimators (Ecam; Siemens Gammasonics). All studies started with the acquisition of a transmission scan using a ^{57}Co-flood source (20% energy window). The transmission measurements had been calibrated in a geometry similar to that used for the volunteers, whereby the transmission was described with the depth-independent buildup factor approach (*15*,*16*). Upon injection of the radioactive tracer, a dynamic study of the thorax and upper abdomen was started (30 frames of 1 min) to visualize the initial activity distribution in the organs with high uptake. Immediately thereafter, a whole-body study was performed, yielding conjugate anterior and posterior views. Additional whole-body scans were acquired at 3, 6, and 24 h after injection. Table speed was 10 cm/min during the first 3 scans and 5 cm/min in the 24-h acquisition. In all studies, the pulse height analyzer was set at 140 keV with a 15% energy window. The volunteers did not leave the table between the dynamic and the first whole-body study at 30 min after injection, so no activity had been lost before the first whole-body scan. This procedure allows the application of the "no-excretion approach" in determining total activity in the body (*16*). Blood samples were taken shortly before injection, frequently during the first hour after injection, and at 2, 3, 4, 6, and 24 h after injection. Urine and feces were collected during the first 24 h. Radioactivity in blood and urine was measured using a γ-counter (1480 Wizard 3″; Wallac). For determination of activity in the feces, the content of the recipient was adjusted to a volume of 500 mL and homogenized. The activity was measured using a 10.16-cm (4 in.) NaI(Tl) scintillation detector and was compared with the activity of a standard solution with the same geometry.

Data Analysis

Total body retention was estimated using the no-excretion approach (*16*), that is, the total counts collected during the first whole-body scan were assumed to correspond to the total injected dose. Total counts from a later whole-body scan at time t_i can be used to estimate total body uptake, or percentage injected dose (%ID), according to uptake(t_i) = (counts(t_i)/counts(first whole-body scan)) × 100%. Counts in this expression are the geometric mean of the anterior and posterior views after correction for background radiation and decay.

To determine organ uptake, regions of interest were defined for all organs showing noticeable uptake, around the bladder, and around a calibrated source that was used to check system stability. The same regions were used in all images of a given volunteer; both copying and mirroring of the regions were thus required. Correction for background radiation was performed according to the method of Buijs et al., which takes finite organ thickness into account (*17*). Absolute organ activity was calculated using the depth-independent buildup factor method according to Siegel et al. (*15*,*16*). This method corrects for attenuation and organ-size–dependent scatter. An estimate of organ thickness, required both for the method of Buijs et al. and for the method of Siegel et al., was obtained as the ratio of organ volume, as given in the MIRD

methodology (*18*), and the area of the region of interest was drawn around the organ. Uptake in the red marrow was derived from activity found in the iliac crests, taking the estimate of Buijs et al. that about 4.4% of all red marrow is present in these locations (*19*). Uptake in an organ was calculated as the decay-corrected activity in that organ, expressed as a percentage or a fraction of the injected dose.

The projections of the liver and right kidney partly overlapped in the anterior and posterior images. The region around the liver was drawn excluding the overlap area, whereas the region around the right kidney included this area. Assuming that, in healthy volunteers, uptake in both kidneys is nearly the same, the amount by which the right kidney uptake is higher than the left kidney uptake gives the overestimation of the right kidney uptake and the underestimation of the liver uptake. Kidney and liver uptake have been corrected accordingly.

Residence times for all organs and the total body were obtained by integrating the time–activity curves, normalized with injected activity but not corrected for physical decay of ^{99m}Tc. For the kidneys, the liver, and the spleen, the time–activity curves were constructed from both the dynamic and the whole-body scans. For the other organs, only data from the whole-body scans could be used, because the dynamic scan covered only part of the thorax and abdomen. In the integration, the available data points were connected with an exponential function, extrapolating the first and last function to times zero and infinity, respectively. Effective half-life ($t_{1/2_{eff}}$), characterizing the disappearance of the activity, was determined by fitting a single exponential curve to the data from the whole-body scans. Biologic half-life ($t_{1/2_{biol}}$) was calculated from $t_{1/2_{eff}}$ and the physical half-life of ^{99m}Tc ($t_{1/2_{phys}}$; 6.007 h) using the relation $(t_{1/2_{eff}})^{-1} = (t_{1/2_{biol}})^{-1} + (t_{1/2_{phys}})^{-1}$.

Quantification of organ uptake and total body retention, residence time, and effective half-life was performed with our own software developed on the Icon computer platform (Siemens Gammasonics). The MIRDOSE3.1 program (*18*) was used to calculate organ doses and effective dose, applying the dynamic bladder model (*20*) with a voiding interval of 4 h and the biologic half-life as measured for that individual.

Safety Parameters

To determine the safety of ^{99m}Tc-HYNIC-AnxV, blood samples were collected and subjected to clinical laboratory chemistry (renal and liver function chemistry, hematology, and blood coagulation parameters). Urine samples were routinely analyzed, including microscopic evaluation. Vital signs including supine blood pressure, pulse, respiration rate, and temperature were checked and a 12-lead electrocardiogram was obtained. Each of these parameters was evaluated at the time of screening of the volunteers, before injection, and at different times after injection of ^{99m}Tc-HYNIC-AnxV.

RESULTS

The mean age of the 6 male volunteers was 23 ± 2 y (range, 21–27 y); their mean body weight was 77 ± 8 kg (range, 64–88 kg). The average injected activity of ^{99m}Tc-HYNIC-AnxV was 254 ± 34 MBq. The overall radiochemical purity was 94.0% ± 1.7%, whereas the percentage of ^{99m}Tc-pertechnetate was 2.0% ± 0.5%. The amount of HYNIC-AnxV protein injected was approximately 25 μg.

None of the volunteers reported any adverse effects, and no changes in the monitored safety parameters were found. Typical examples of the activity distribution in one of the volunteers at 30 min and 24 h after injection are shown in Figure 1. Note the very high uptake in the kidneys and the lack of activity in the gut even at 24 h after injection. The estimated activity was higher in the right kidney than in the left kidney (on average, 1.1 ± 0.6 %ID). This difference was attributed to

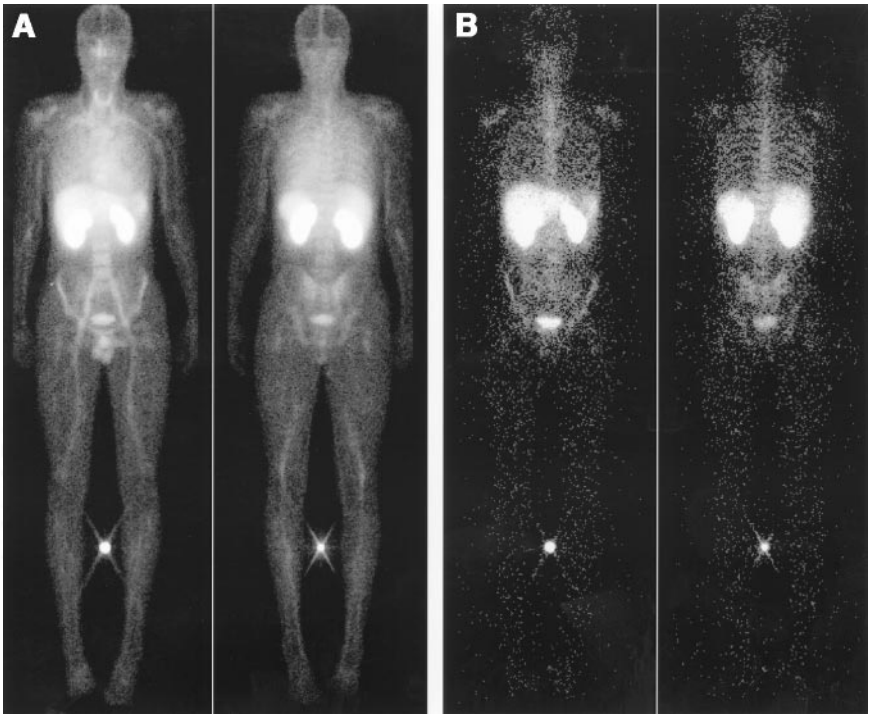

FIGURE 1. Conjugate views from whole-body scans of 22-y-old male volunteer. Scans were acquired at about 30 min (A) and 24 h (B) after intravenous injection of 263 MBq of ^{99m}Tc-HYNIC-AnxV. In each pair, anterior view is on left and posterior view is on right.

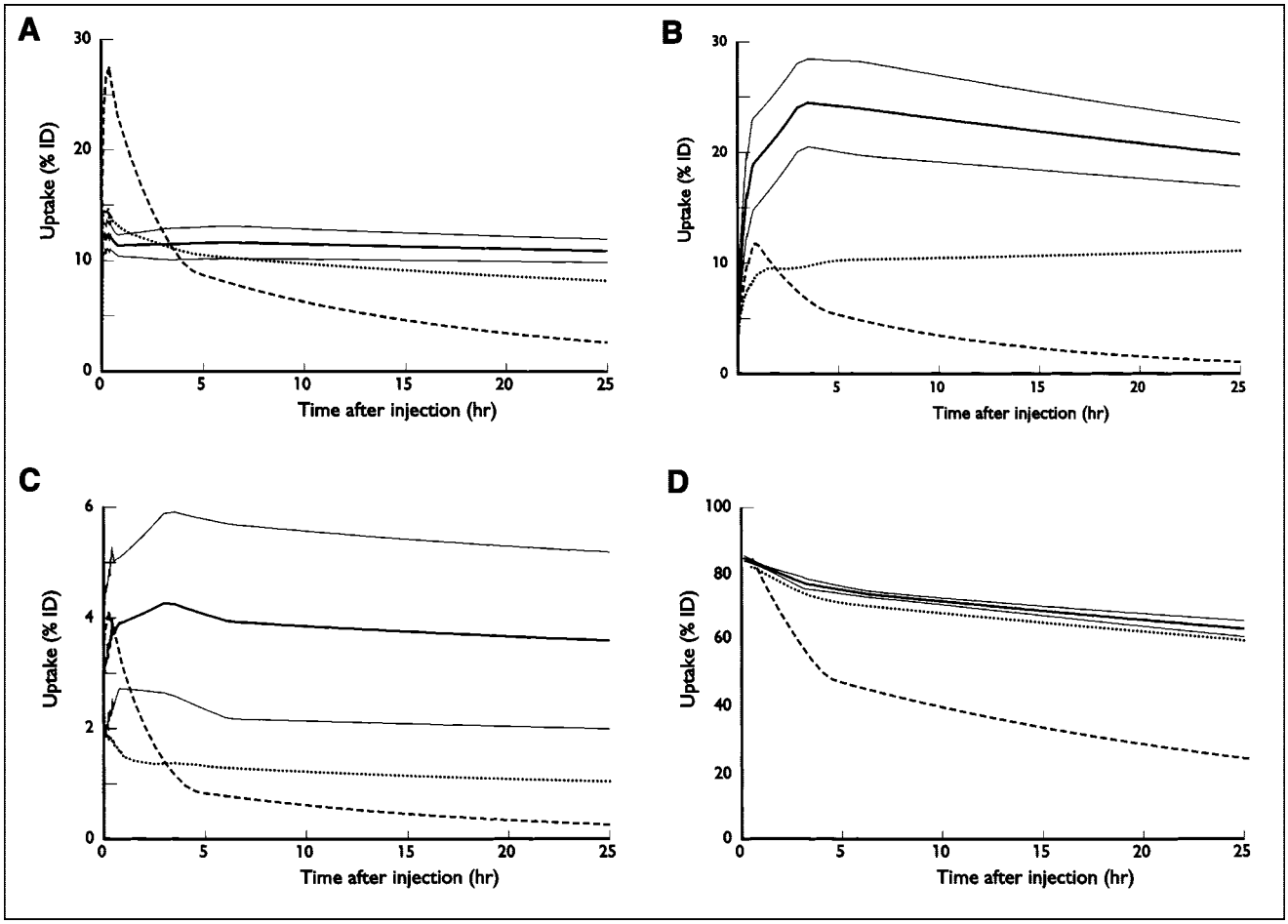

FIGURE 2. Decay-corrected ^{99m}Tc uptake vs. time curves for liver (A), left kidney (B), spleen (C), and total body (D) after intravenous injection of ^{99m}Tc-HYNIC-AnxV. Curves representing mean (thick line) and mean ± 1 SD (thin lines) are shown. For comparison, curves representing average uptake for ^{99m}Tc-i-AnxV (dotted line) and ^{99m}Tc-BTAP-AnxV (dashed line) from previous studies are also shown (*9,10*).

overlap of the right kidney and the liver in the anterior and posterior images and was used to improve the estimates of kidney and liver uptake. Apart from the kidneys, the liver and the spleen also had considerable uptake. Some activity also visibly concentrated in the skeleton, most likely in the red marrow (range, 6.4–11.2 %ID at 3 h after injection). In most cases, the thyroid could also be seen, but no significant correlation between thyroid uptake and percentage of pertechnetate in the injected preparation was found.

Figure 2 shows the average uptake and the uptake ± the SD as a function of time for the organs with high uptake and for the total body. The average uptake curves for the 2 previously studied radiopharmaceuticals (^{99m}Tc-i-AnxV and ^{99m}Tc-BTAP-AnxV) are also shown for comparison (*9,10*). The uptake in the liver and the spleen did not change much over time. The same held true for the activity in the red bone marrow (on average, 0.085, 0.092, 0.090, and 0.090 %ID at 30 min, 3 h, 6 h, and 24 h, respectively, after injection).

Pharmacokinetic parameters of decay-corrected ^{99m}Tc-activity in blood and plasma during the first 24 h after injection are shown in Table 1. Fitting with a 2-compartment model resulted, in all cases, in a satisfactory description of clearance of activity from the blood. The small and slowly cleared compartment (β) is characterized by a much longer half-life than the large α-compartment.

Figure 3 presents the cumulative excretion of ^{99m}Tc-HYNIC-AnxV in the urine. During the first 24 h after injection, 22.5 ± 3.5 %ID had been excreted in the urine and 0.11 ± 0.18 %ID in the stool, totaling 22.6 ± 3.5 %ID, which agrees well with the estimate from the whole-body scans (23.4 ± 2.2 %ID). Because the fraction of the activity

TABLE 1
Pharmacokinetic Parameters of Decay-Corrected ^{99m}Tc-Activity in Blood and Plasma During First 24 Hours After Injection of HYNIC-AnxV in 6 Volunteers

	α (fast) component		β (slow) component	
Measurement	t½ (min)	Fraction	t½ (h)	Fraction
Blood	24 ± 3	0.92 ± 0.03	35 ± 44	0.08 ± 0.03
Plasma	27 ± 7	0.91 ± 0.02	41 ± 53	0.09 ± 0.02

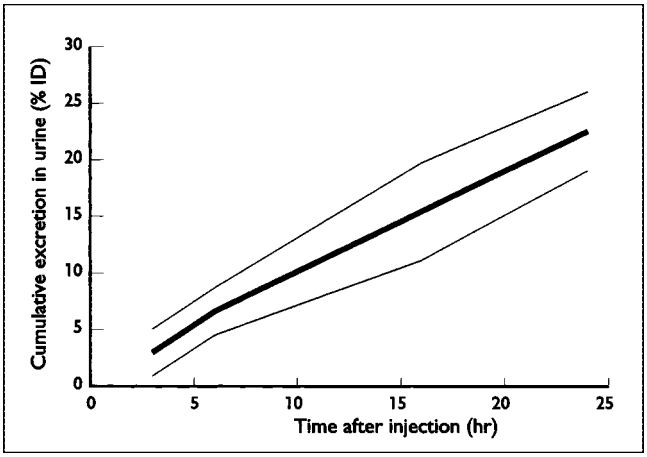

FIGURE 3. Cumulative excreted activity in urine (decay corrected). Curves representing mean (thick line) and mean ± 1 SD (thin lines) are shown.

leaving the body through the feces was small, we assumed, for the dynamic bladder model, that all activity was cleared by the kidneys.

A summary of dosimetric parameters for various organs and total body is given in Table 2. The uptake is shown at 3 h after injection, a time at which the accumulation of activity in the kidneys, the liver, and the spleen is probably close to its highest value. The kidneys clearly had the highest uptake and the highest absorbed dose. Although the study involved only men, MIRDOSE3.1 also gives an estimate of the dose in ovaries if these had been present (3.1 ± 0.3 μGy/MBq).

DISCUSSION

^{99m}Tc-HYNIC-AnxV had a favorable biodistribution that may allow imaging of apoptosis nearly everywhere in the body, with the exception of the kidneys, the liver, and the spleen. Little activity accumulated outside these organs and more than 90% of blood activity was cleared with a short half-life of about 25 min. Interestingly, the bowel remained clear of activity at least up to 24 h after injection, indicating that visualization of apoptotic processes in the abdomen should be feasible. This finding is in sharp contrast to the findings for ^{99m}Tc-BTAP-AnxV and ^{99m}Tc-i-AnxV. In the case of ^{99m}Tc-BTAP-AnxV, activity was visible in the gut at 4 h after injection (*10*), whereas in the case of ^{99m}Tc-i-AnxV, gut activity appeared somewhere between 4 and 20 h after injection (*9*).

Another advantage of ^{99m}Tc-HYNIC-AnxV is the ease of its preparation, taking less than about 30 min, with good radiochemical purity (94.0% ± 1.7%) and low amounts of free pertechnetate (2.0% ± 0.5%). The remaining 4% of ^{99m}Tc impurities is present as ^{99m}Tc-tricine, possibly with traces of ^{99m}Tc-glycyl-HYNIC or colloidal ^{99m}Tc. In contrast to HYNIC, the preparation of ^{99m}Tc-BTAP-AnxV is extremely elaborate, whereas for ^{99m}Tc-i-AnxV the purity was generally rather low (82% ± 12%).

Because of the long biologic half-life, the effective dose (11.0 ± 0.8 μSv/MBq)) of ^{99m}Tc-HYNIC-AnxV is in the high range of values for commonly used ^{99m}Tc-radiopharmaceuticals (*21*). Uptake of activity in the kidneys was high (49.7 ± 8.1 %ID), comparable to what has been reported by Ohtsuki et al. for Sprague–Dawley rats (47.4 ± 2.9 %ID at

TABLE 2
Dosimetric Data for Intravenously Administered ^{99m}Tc-HYNIC-AnxV

Site	Uptake* (%ID)	Effective half-life† (h)	Residence time (h)	Absorbed dose (μGy/MBq)	Absorbed dose, Apomate‡ (μGy/MBq)	Absorbed dose, ^{99m}Tc-i-AnxV§ (μGy/MBq)
Kidneys	49.7 ± 8.1‖	5.9 ± 0.1	3.90 ± 0.63	196 ± 31	63 ± 22	93 ± 24
Liver	13.1 ± 1.0‖	5.9 ± 0.1	1.03 ± 0.10	16.9 ± 1.3	13 ± 3	17 ± 2
Red bone marrow	9.2 ± 1.8	6.0 ± 0.1	0.78 ± 0.15	8.4 ± 0.9	4.0 ± 0.7	5.5 ± 0.8
Spleen	4.6 ± 1.6	5.7 ± 0.4	0.36 ± 0.13	41 ± 12	15 ± 3	22 ± 6
Testes (n = 6)	0.16 ± 0.04	4.6 ± 0.3	0.014 ± 0.003	5.3 ± 0.9	6.3 ± 1.6	15 ± 3
Thyroid	0.14 ± 0.08	4.4 ± 0.7	0.011 ± 0.005	7.1 ± 3.2	5.6 ± 3.6	10 ± 6
Urinary bladder¶	—	—	0.15 ± 0.01	7.5 ± 0.4	20 ± 6	7.5 ± 2.6
Remainder	—	—	1.58 ± 0.81	—	—	—
Total body	91.6 ± 1.7	5.5 ± 0.1	7.82 ± 0.08	11.0 ± 0.8#	7.6 ± 0.5#	9.7 ± 1.0#

*Uptake values are at 3 h after injection and are corrected for physical decay.
†Results are from a fit with a single exponential.
‡(*10*).
§(*9*).
‖Including correction for overlap between right kidney and liver; see text.
¶Dynamic bladder model (*20*); 4-h voiding interval; biologic half-life of activity in total body from individual measurements (average, 69 ± 7 h); fraction of activity to urine = 1.0.
#Effective dose (ICRP 60) in μSv/MBq.
Data are mean ± SD (n = 6).

3 h after injection) (*12*). The kidney absorbed dose was relatively high too—196 ± 31 μGy/MBq—but slightly lower than reported by Steinmetz et al. (0.23 mSv/MBq) (*22*). According to the present study, the mean injected activity of 250 MBq would cause an organ dose of about 49 mGy. The threshold for nephrotoxicity depends on the time course of the irradiation. For tolerance dose 5/5 (the probability of 5% complications within 5 y of irradiation), Emami et al. reported 14 Gy when delivering the radiation dose in 2 fractions and 28 Gy when using 25 fractions (*23*). Clearly, the dose is not likely to exceed the threshold for nephrotoxicity, even if several investigations were performed over time with a higher injected activity (up to about 740 MBq, as with other ^{99m}Tc compounds). The uptake of activity in the red bone marrow was relatively high, an observation corresponding to the results obtained by Ohtsuki et al. in rats. These authors suggested that the bone marrow uptake was physiologic, since apoptotic cell death is a physiologic component of normal hematopoiesis (*12*).

Uptake in the thyroid (0.14 ± 0.08 %ID) was clearly visible in some of the volunteers. However, both previously studied compounds showed an even slightly higher thyroid uptake: 0.21 ± 0.11 %ID for ^{99m}Tc-i-AnxV and 0.28 ± 0.12 %ID for ^{99m}Tc-BTAP-AnxV. No significant correlation was found between the percentage of pertechnetate in the injected preparation and thyroid uptake. Because of the uncertainty in the estimated thyroid activity caused by the relatively large background correction for this organ, we also looked for a correlation between pertechnetate concentration and the uncorrected thyroid activity. No significant correlation was found in that case either.

Finally, ^{99m}Tc-HYNIC-AnxV was found to be a safe radiopharmaceutical in this study because none of the volunteers reported any adverse effect and no changes were observed in any of the safety parameters obtained before and after administration.

CONCLUSION

The results of this study have indicated that ^{99m}Tc-HYNIC-AnxV is a safe radiopharmaceutical with a favorable biodistribution and acceptable radiation burden. Therefore, additional clinical studies are now under way to evaluate the utility of performing ^{99m}Tc-HYNIC-AnxV imaging of apoptosis in patients.

ACKNOWLEDGMENT

The authors thank Prof. Dr. Guido A.K. Heidendal, head of the Department of Nuclear Medicine in Maastricht, for valuable contributions to this work.

REFERENCES

1. Gastman BR. Apoptosis and its clinical impact. *Head Neck.* 2001;23:409–425.
2. Blankenberg FG, Tait JF, Strauss HW. Apoptotic cell death: its implications for imaging in the next millennium. *Eur J Nucl Med.* 2000;27:359–367.
3. Blankenberg FG, Strauss HW. Will imaging of apoptosis play a role in clinical care? A tale of mice and men. *Apoptosis.* 2001;6:117–123.
4. Reutelingsperger CPM, Dumont E, Thimister PW, et al. Visualization of cell death in vivo with the annexin A5 imaging protocol. *J Immunol Methods.* 2002;265:123–132.
5. Fadok VA, Voelker DR, Campbell PA, Cohen JJ, Bratton DL, Henson PM. Exposure of phosphatidylserine on the surface of apoptotic lymphocytes triggers specific recognition and removal by macrophages. *J Immunol.* 1992;148:2207–2216.
6. Reutelingsperger CPM, Kop JMM, Hornstra G, Hemker HC. Purification and characterization of a novel protein from bovine aorta that inhibits coagulation: inhibition of the phospholipid-dependent factor-Xa-catalyzed prothrombin activation, through a high-affinity binding of the anticoagulant to the phospholipids. *Eur J Biochem.* 1988;173:171–178.
7. Martin SJ, Reutelingsperger CPM, McGahon AJ, et al. Early redistribution of plasma membrane phosphatidylserine is a general feature of apoptosis regardless of the initiating stimulus: inhibition by overexpression of Bcl-2 and Abl. *J Exp Med.* 1995;182:1545–1556.
8. Hofstra L, Liem IH, Dumont EA, et al. Visualisation of cell death in vivo in patients with acute myocardial infarction. *Lancet.* 2000;356:209–212.
9. Kemerink GJ, Liem IH, Hofstra L, et al. Patient dosimetry of intravenously administered ^{99m}Tc-annexin V. *J Nucl Med.* 2001;42:382–387.
10. Kemerink GJ, Boersma HH, Thimister PWL, et al. Biodistribution and dosimetry of ^{99m}Tc-BTAP-annexin-V in humans. *Eur J Nucl Med.* 2001;28:1373–1378.
11. Blankenberg FG, Katsikis PD, Tait JF, et al. In vivo detection and imaging of phosphatidylserine expression during programmed cell death. *Proc Natl Acad Sci USA.* 1998;95:6349–6354.
12. Ohtsuki K, Akashi K, Aoka Y, et al. Technetium-99m HYNIC-annexin V: a potential radiopharmaceutical for the in-vivo detection of apoptosis. *Eur J Nucl Med.* 1999;26:1251–1258.
13. Blankenberg FG, Katsikis PD, Tait JF, et al. Imaging of apoptosis (programmed cell death) with ^{99m}Tc annexin V. *J Nucl Med.* 1999;40:184–191.
14. Blankenberg FG, Strauss HW. Non-invasive diagnosis of acute heart- or lung-transplant rejection using radiolabeled annexin V. *Pediatr Radiol.* 1999;29:299–305.
15. Siegel JA. The effect of source size on the buildup factor calculation of absolute volume. *J Nucl Med.* 1985;26:1319–1322.
16. MIRD pamphlet no 16: techniques for quantitative radiopharmaceutical biodistribution data acquisition and analysis for use in human radiation dose estimates. *J Nucl Med.* 1999;40:37S–61S.
17. Buijs WCAM, Siegel JA, Boerman OC, Corstens FHM. Estimation of absolute organ activity using five different methods of background correction. *J Nucl Med.* 1998;39:2167–2174.
18. Stabin MG. MIRDOSE: personal computer software for internal dose assessment in nuclear medicine. *J Nucl Med.* 1996;37:538–546.
19. Buijs WC, Oyen WJ, Dams ET, et al. Dynamic distribution and dosimetric evaluation of human non-specific immunoglobulin G labelled with ^{111}In or ^{99}Tc^{m}. *Nucl Med Comm.* 1998;19:743–751.
20. Cloutier R, Smith S, Watson E, Snyder W, Warner G. Dose to the fetus from radionuclides in the bladder. *Health Phys.* 1973;25:147–161.
21. *Radiation Dose to Patients from Radiopharmaceuticals: Addendum to ICPR Publication 53.* Oxford, U.K.: Pergamon Press; 1998:113–120. ICRP publication 80.
22. Steinmetz ND, Green AM, Sparks RB, Vanderheyden J-L. Safety, tolerability, biodistribution, and radiation dosimetry of Tc-99m-hynic-annexin [abstract]. *Eur J Nucl Med.* 2002;29(suppl 1):S49.
23. Emami B, Lyman J, Brown A, et al. Tolerance of normal tissue to therapeutic irradiation. *Int J Radiat Oncol Biol Phys.* 1991;21:109–122.